applied optics

All-fiber laser system for all-optical ^{87}Rb Bose Einstein condensate to space application

Lin Li,[1,2,3] Cuiyun Zhou,[1] Wei Xiong,[4] Minjie Huang,[1] Su Fang,[1] Xingping Xu,[1] Jingwei Ji,[1] Min Gao,[1] Tieqiang Song,[1,3] Yi Hong,[1] Zhaogang Liang,[1] Dijun Chen,[1] Xia Hou,[1] Xiaoji Zhou,[4] Xuzong Chen,[4] Weibiao Chen,[1] Bin Wang,[1,5,†] Tang Li,[1,6,†] and Liang Liu[1,2,*]

[1]Spaceborne Laser Engineering Department, Shanghai Institute of Optics and Fine Mechanics, Chinese Academy of Sciences, Shanghai 201800, China
[2]Key Laboratory of Quantum Optics and Center of Cold Atom Physics, Shanghai Institute of Optics and Fine Mechanics, Chinese Academy of Sciences, Shanghai 201800, China
[3]Center of Materials Science and Optoelectronics Engineering, University of Chinese Academy of Sciences, Beijing 100049, China
[4]School of Electronics, Peking University, Beijing 100871, China
[5]wangbin@siom.ac.cn
[6]litang@siom.ac.cn
[†]These authors contributed equally to this work.
*liang.liu@siom.ac.cn

Received 12 June 2023; revised 19 September 2023; accepted 21 September 2023; posted 25 September 2023; published 9 October 2023

In the development of the Cold Atom Physics Research Rack (CAPR) on board the Chinese Space Station, the laser system plays a critical role in preparing the all-optical ^{87}Rb Bose–Einstein condensates (BECs). An all-fiber laser system has been developed for CAPR to provide the required optical fields for atom interaction and to maintain the beam pointing in long-term operation. The laser system integrates a 780 nm fiber laser system and an all-fiber optical control module for sub-Doppler cooling, as well as an all-fiber 1064 nm laser system for evaporative cooling. The high-power, single-frequency 780 nm lasers are achieved through rare-Earth doped fiber amplification, fiber frequency-doubling, and frequency stabilization technology. The all-fiber optical control module divides the output of the 780 nm laser system into 15 channels and regulates them for cooling, trapping, and probing atoms. Moreover, the power consistency of each pair of cooling beams is ensured by three power tracking modules, which is a prerequisite for maintaining stable MOT and molasses. A high-power, compact, controlled-flexible, and highly stable l064 nm all-fiber laser system employing two-stage ytterbium-doped fiber amplifier (YDFA) technology has been designed for evaporative cooling in the optical dipole trap (ODT). Finally, an all-optical ^{87}Rb BEC is realized with this all-fiber laser system, which provides an alternative solution for trapping and manipulating ultra-cold atoms in challenging environmental conditions.

https://doi.org/10.1364/AO.497749

1. INTRODUCTION

The achievement of Bose–Einstein condensates (BECs) through evaporative cooling in magnetic and optical dipole traps is a milestone in the realm of quantum mechanics [1–4]. It serves as a paradigm for investigating quantum precision measurement [5,6] and interactions in quantum systems [7–9] because of the high phase-space density (PSD) and strong space-time coherence properties. However, the investigation is subject to the gravitation influence, resulting in atoms accumulating at the bottom of the potential well, leakage from the trap, and departure from the observed potential field [10,11], which greatly restricts its observation and application. In microgravity, atoms can be cooled to pico-kelvin or even femto-kelvin using the trap frequencies in the hertz regime [12,13]. The atoms can be observed for hundreds of milliseconds, or even seconds, in a weightlessness environment. This is a challenging task for compact cold atom systems within an Earth-bound laboratory [14]. It has greatly stimulated the enthusiasm for cold atom research in microgravity and facilitated the advancement of state-of-the-art ultra-cold experiments on various microgravity research platforms, such as drop towers, Einstein elevators, zero-g flights, and sounding rockets, as well as the International Space Station (ISS) [15–20].

The CAPR has been deployed on the Chinese Space Station (CSS) to explore the artificial lowest temperature and quantum simulation of BEC in microgravity, taking advantage of the inherent benefits of weightlessness. Developing a highly reliable and versatile laser system for preparing all-optical ^{87}Rb BEC is

one of the most challenging tasks for CAPR. Two laser systems are required, with the first being closely resonant with rubidium atoms to cool them to micro-kelvin and probe them, while the second is far-off resonant for trapping and evaporative cooling of the atoms to degenerate. The laser system must be reliable and maintain its performance despite the vibrations and impacts experienced during launch. In order to manipulate atoms in space while meeting the constrains of size, weight, and power consumption (SWaP), high demands are placed on the laser system with regards to miniaturization, power consumption, and thermal stability. In addition to performing complex control procedures for all lasers used in ultra-cold atom experiments, a flexible control manner of lasers is necessary considering the experimental sequence being ultimately received via a space-to-ground communication link. An all-fiber laser system presents a promising solution for achieving the all-optical ^{87}Rb BEC in the CSS, owing to its inherent advantages such as its lightweight design, ease of integration and transport, and robustness against mechanical and thermal perturbations.

However, up to now, the polarization maintenance of 780 nm fused fiber devices is less reliable [21,22] for sub-Doppler cooling and atom probing in a challenging environment. To date, there have been no reports of an all-fiber laser system capable of efficiently trapping and evaporatively cooling in the ODT. Mainstream laser system solutions for cold atom research and application in harsh environments rely on the integrated, compact, and robust free-space optical benches based on materials with excellent mechanical thermal stability, like SiC-reinforced Al-Si alloy and ZERODUR [23–25], or in conjunction with commercial fiber telecom technologies. With the advancements in the erbium-doped fiber amplifier (EDFA) and fiber-pigtailed periodically poled lithium niobate (PPLN) technologies, the telecom fiber laser system [26–28] becomes an alternative technical for atoms cooling, trapping, and detecting in out-of-the lab environments [29–33]. The reliability of the commercial fiber telecom technologies and integrated free-space optical benches has been demonstrated through experiments conducted aboard a parabolic flight [34,35], in the sounding rocket [36–41] and the ISS [42,43].

Here, we present the design, realization, and validation of the all-fiber laser system for CAPR, which consists of a 780 nm laser system, an optical control module, and a 1064 nm laser system. The 780 nm fiber laser system comprises a repumping laser, a cooling laser, and a probing laser, which provides three high-power outputs for cycling cooling the ^{87}Rb atoms to tens of microkelvin and detecting them. The optical control system divides the 780 nm laser system into 15 optical modules. These modules are mounted on the vacuum apparatus [44] and provide the necessary optical fields for atom interaction. The 1064 nm all-fiber laser system serves as a high-power, compact, controlled-flexible, and highly stable laser source for ODT and evaporative cooling to BEC. The paper is organized as follows. The 780 nm laser system is demonstrated in Section 2. With the utilization of modulation transfer spectroscopy (MTS) [45] and optical phase-locked loops (OPLL), all 780 nm lasers exhibit a frequency stability below 4×10^{-11} for integration times ranging from 1 to 1000s. The optical control system is described in Section 3. The power tracking module significantly mitigates the power fluctuation of the 3D-MOT cooling beams, reducing the difference between each pair of counter-propagating cooling beams by an order of magnitude. Section 4 illustrates the realization of a high-power, compact, and all-fiber 1064 nm laser system through two-stage YDFA technology. Both the open-loop configuration of the second stage fiber amplifiers and the closed-loop management of the acousto-optic modulators (AOMs) are effective power control strategies that contribute to the stability and adjustment precision during evaporative cooling. The optical performance of the all-fiber laser system is functionally validated through efficient cooling of atoms to tens of microkelvin and further evaporative cooling to BEC. Section 5 provides a detailed account of the cooling process. The conclusion is given in Section 6.

2. 780 nm LASER SYSTEM

For cooling the ^{87}Rb atoms in microgravity, a 780 nm fiber laser system has been developed based on telecom fiber amplifier technology, second harmonic generation (SHG) technology, frequency stabilization, and phase locking technology, as shown in Fig. 1.

Typically, two 780 nm laser lines are required for cooling, trapping, and probing the ^{87}Rb atoms. The first one, in order to cool and probe the atoms, is red-detuned by a few Γs ($\Gamma = 2\pi \times 6.065(9)$ MHz, the natural linewidth of the ^{87}Rb D_2 line) from the ^{87}Rb D_{2a} $|5^2S_{1/2}, F = 2\rangle \rightarrow |5^2P_{3/2}, F' = 3\rangle$ transition. The second one, referred as the repumping laser, is resonant with the transition from D_{2b} $|5^2S_{1/2}, F = 1\rangle$ to $|5^2P_{3/2}, F' = 2\rangle$ of ^{87}Rb and is employed to pump atoms out of the dark state $|5^2S_{1/2}, F = 1\rangle$.

As depicted in Fig. 1, the repumping laser is locked to the ^{87}Rb D_{2b} $|5^2S_{1/2}, F = 1\rangle \rightarrow |5^2P_{3/2}, F' = 0, 1\rangle$ crossover transition via MTS, which is 193 MHz red-detuned from the repumping transition. The seed laser of repumping laser is used as a fixed frequency reference for other two seed lasers. By utilizing OPLLs, both the cooling laser and probing laser are frequency locked onto the reference. Therefore, the cooling laser and probing laser can be manipulated their detuning from 0 to -20Γ to ^{87}Rb D_{2a} $|5^2S_{1/2}, F = 2\rangle \rightarrow |5^2P_{3/2}, F' = 3\rangle$ transition.

The output power of repumping laser, cooling laser, and probing laser is 200 mW, 600 mW, and 800 mW, respectively. These lasers employ similar optical schemes. Starting from the 1560 nm distributed feedback (DFB) laser (Emcore, 1782), all the 780 nm lasers are generated by erbium-doped fiber (Coractive, DCF-EY-10/128-PM) and a following PM fiber pigtailed wave-guide-type PPLN crystal (NTT Electronics, WH-0780-000-F-B-C-M). The fiber optical isolators in the laser system serve to safeguard the DFB lasers and EDF amplifiers from any potential optical feedback. The seeding source is amplified by the pumping diode laser (BWT, K940EB2RN-10.00 W), and the unabsorbed pumping light is damped by strippers. The ability to adjust the power of cooling and probing lasers is realized via tuning the pump current of the pumping diode laser. The switch-off of the cooling laser and probing laser is achieved by turning off the pumping current and the optical switch (Primanex, RFMS10-12PMR1C21122) before the EDF

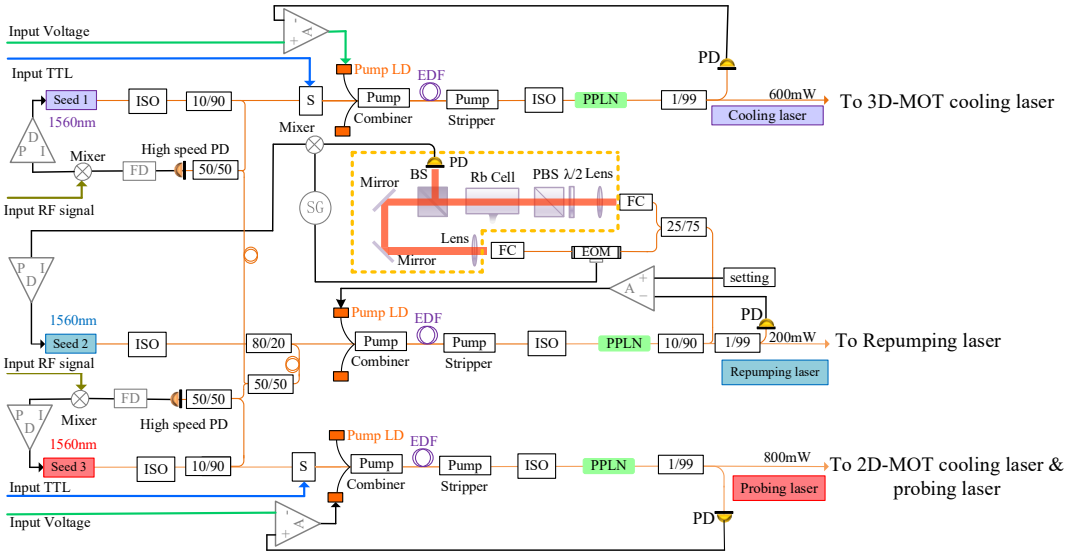

Fig. 1. Scheme of the 780 nm lasers, including the repumping laser, the cooling laser, and the probing laser. ISO, isolator; FS, fiber splitter; S, shutter; EDF, erbium-doped fiber; PPLN, periodically poled lithium niobate; FC, fiber collimator; EOM, electro-optic modulator; PD, photodiode; BS, beam splitter; SG, signal generation; FD, frequency divider; PID, proportional integral differential.

amplifier. The switch-off time is 50 μs, and the on-off extinction ratio is over 120 dB.

A FS divides 10% power of the 780 nm repumping laser for MTS to stabilize its frequency. The MTS module, which is in the yellow dotted area in Fig. 1, is the only free-space optical component within this fiber laser system. A FS splits the MTS power into two parts, allocating 75% for pumping light and 25% for probing light. Each portion is then transmitted through a fiber collimator and lens to free-space. The photodiode (PD) is utilized to monitor the MTS signal of the probing light. A frequency mixer is used to generate the error signal from the amplified PD signal and the modulation signal for the fiber electro-optic modulator (EOM). The proportional integral differential (PID) circuit filters the mixer output and sends it back to the seeding source for laser clocking. Additionally, 20% power of the seed 2 (seed 2 is the laser source of the repumping laser as shown in Fig. 1) is split for frequency locking the other two 780 nm lasers via OPLLs. The fiber coupled packaged high-speed photodiode detects the beat signal of seed 1 and seed 2, seed 2 and seed 3, respectively. Two beat signals are phase-locked to two independent tunable RF references so that the frequency of cooling laser and probing laser can be adjusted. The frequency stabilities of the three 780 nm lasers are evaluated by comparing their output to the optical frequency comb depicted in Fig. 2. All the lasers can be locked for a very long time with a characteristic drift over 3600 s of around 50 kHz. Figure 2 displays the Allan deviation of the beat note acquired by the counter, demonstrating frequency stability below 4×10^{-11} with integration time from 1 s to 1000 s.

We incorporate a FS into each laser output to allocate one percent of the power for monitoring purpose. The primary purpose is to record real-time power to assess the performances of the lasers. The secondary goal is to establish a servo loop for power locking by manipulating the pump current, achieving the power fluctuation of less than 1% (peak to peak) over a period of 1 h.

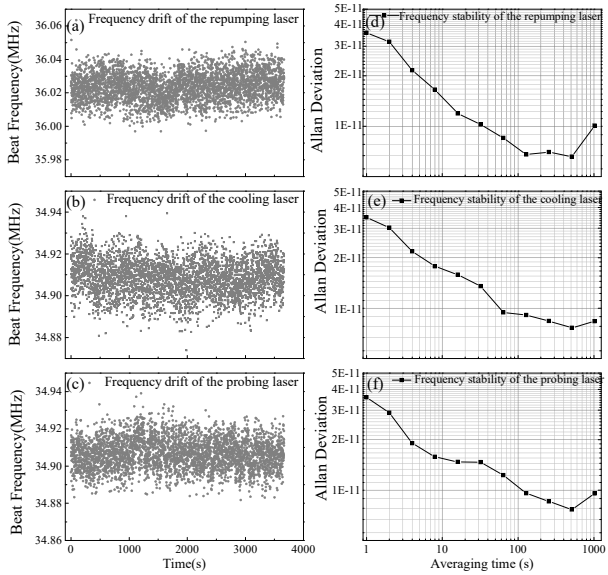

Fig. 2. Beat note frequency between the optical frequency comb (OFC) and (a) the repumping laser, (b) the cooling laser, and (c) the probing laser. The corresponding Allan deviation of these samples is shown in (d)–(f), respectively.

3. OPTICAL CONTROL SYSTEM

The 780 nm laser system is connected to many PM fibers for different applications, which is summarized in the all-fiber optical control system shown in Fig. 3. The splitters, combiners, AOM, attenuators, and shutters pigtailed with PM fiber actualize all the power controlling, the frequency manipulation, and the switch requirements. The optical control module has 15 output ports for atom cooling and probing, all of which are connected to the vacuum system via PM fiber. These outputs consist of one 2D magneto-optical trap (MOT) repumping beam, two 3D MOT

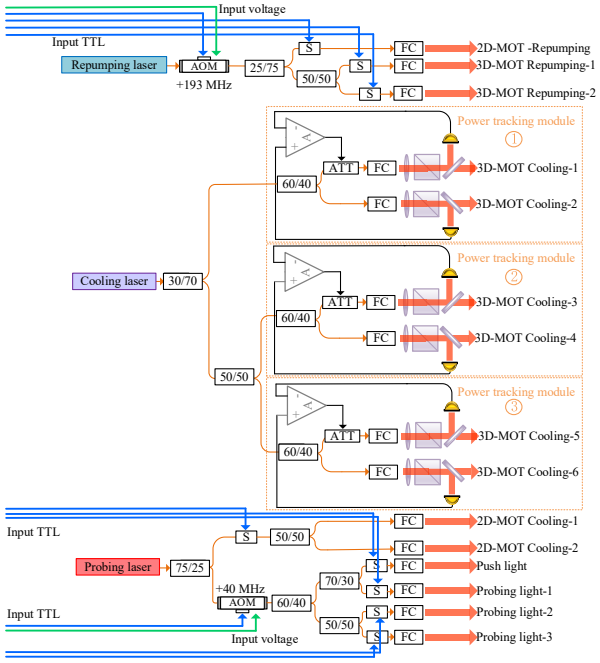

Fig. 3. Scheme of the optical control module, including all the 780 nm beams transferred to the physical system. AOM, acousto-optic modulator; ATT, attenuator.

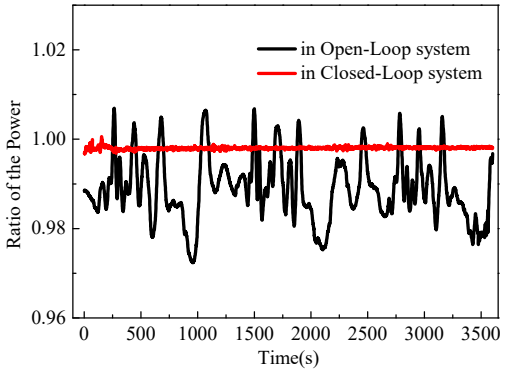

Fig. 4. Ratio of the power of two beams in one pair of counter-propagating cooling beams during 1 h while the power locking module is on and off.

repumping beams, two 2D MOT cooling beams, six 3D MOT cooling beams, one pushing beam, and three probing beams.

After being modulated by the AOM (+193 MHz, in-house made), the repumping laser frequency is resonant with the ^{87}Rb D_{2b} $|5^2S_{1/2}, F = 1\rangle \rightarrow |5^2P_{3/2}, F' = 2\rangle$ repumping transition. The power and the switch of the repumping laser can be independently controlled via the AOM. The repumping laser is divided into three portions through two FSs, as the 2D-MOT repumping, the 3D-MOT repumping-1, and the 3D-MOT repumping-2. In addition, each repumping laser passes a shutter (PMMEMSSW-78-1-2-L-1, SR19761, Advanced Fiber Resources) with a switching time of less than 1 ms. The entire optical control system's output power is displayed in Table 1.

Five FSs with the fixed splitting ratio separate the cooling laser into six outputs, which corresponds to three pairs $\sigma^+ \sigma^-$ circularly polarized beams for 3D-MOT and molasses. It is a challenge for such a multifunctional all-fiber optical control system to maintain high-power stability and high-polarization stability. There are many external factors that lie beyond our control, such as the splitting ratio of the FS, inconsistent insertion loss of fiber components, and the different sensitivity of the fiber components to the environment such as vibration and temperature drift. To maintain power consistency of each pair of cooling beams and achieve a stable atomic cloud in 3D-MOT, three power tracking modules are utilized for each pair of cooling beams. Each cooling beam is detected by a PD, and the power of the counter-propagating cooling beams pair is close-loop locked based on feedback signals from the PDs, utilizing a fiber attenuator (OZ optics MMVOA-1-780-P-5/125-3 A-900-1) in the path of one beam. The position of power sampling is located behind a polarizing beam splitter, in the optical module mounted to the vacuum system, so that both the power instability and the polarization instability will be transferred to the power fluctuation. With the consideration of a 1.5 dB insertion loss caused by the attenuator, we recommend a splitting ratio of 6:4 for each pair of counter-propagating cooling beams. The power ratio fluctuation between two beams in one counter-propagating pair is illustrated in Fig. 4. The peak-to-peak value of the power ratio changes from 1.0345 to 1.00385 when the closed-looped system is switched on. The power difference between counter beams has been reduced by an order of magnitude, decreasing from 3.45% to 0.385% with the power locking module.

Table 1. Output Power of Each Fiber in the Optical Control System

Fiber	Output Power (mW)
2D-MOT repumping	20.7
3D-MOT repumping 1	32.2
3D-MOT repumping 2	30.2
3D-MOT cooling 1	73.1
3D-MOT cooling 2	64.0
3D-MOT cooling 3	88.5
3D-MOT cooling 4	67.8
3D-MOT cooling 5	84.4
3D-MOT cooling 6	66.6
2D-MOT cooling 1	196.8
2D-MOT cooling 2	195.0
Pushing light	11.0
Probing light 1	11.5
Probing light 2	10.8

4. 1064 nm LASER SYSTEM

We intend to develop an all-fiber 1064 nm laser system for preparing the quantum degenerate gases in microgravity, and we summarize the requirements as follows: (i) In order to trap enough atoms in the ODT, the output power and the beam waist of the laser have to be sufficient to form a deep and big enough trap to load atoms from the molasses; (ii) the power and direction of ODT beams should be highly stable to reduce the atom losses; (iii) for effective evaporation, the 1064 nm laser system is required to adjust the ODT depth precisely in a large dynamic range while maintain its power stability; (iv) the laser

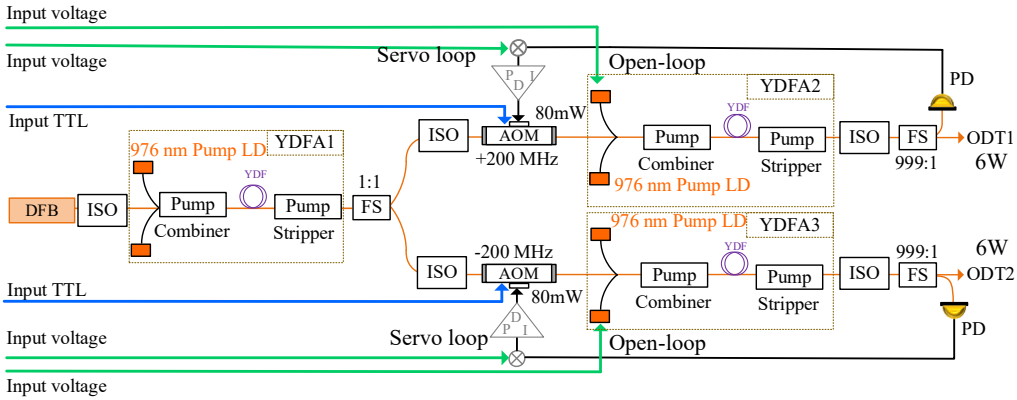

Fig. 5. Sketch of the all-fiber 1064 nm laser system. DFB, distributed feedback laser; ISO, fiber optical isolator; YDF, ytterbium-doped fiber; FS, fiber splitter; AOM, acousto-optic modulator; PID, proportional integral differential; LD, laser diode; PD, photodiode.

output can be turned off in 1 ms to avoid the reshaping of atomic cloud in the turn off process of ODT.

As shown in Fig. 5, we demonstrate an all-fiber high-power 1064 nm laser system with two independent outputs (ODT 1 and ODT 2). A two-stage YDFA structure is adopted for the high-power output, the Yb-doped gain fiber is from Coherent (Nufern, PM-YSF-HI-HP), and each output has maximum power of 6 W. The DFB seeding source (QD laser, QLD1061) and the first-stage amplifier (YDFA 1) are commonly used, which makes the laser system more compact. The output of the YDFA 1 is 500 mW, and it is split equally by the fiber splitter and shifted with two AOMs (in-house made) by different frequencies (−200 MHz and +200 MHz, respectively). After being amplified by the second-stage amplifiers (YDFA 2 and YDFA 3), the laser outputs are shaped and focused by the optical modules to form ODT beams in the science chamber and used for forced evaporation process. FSs are inserted into each output channel for power sampling, and it is also used for power controlling with closed-loop mode.

The effective evaporation was executed by ramping down the power of the 1064 nm laser. Here, the laser power is controlled by both the second-stage amplifier and the AOM. The regulated output power of the 1064 nm laser is shown in Fig. 6. The output power versus the injected current of YDFA is shown in Fig. 6(a), the maximum output power is 6 W at 4.5 A pump current, and the output power is 80 mW when the pump current is below the threshold. When the laser's power ranges from 6 W to 80 mW, an open-loop control strategy was adopted via controlling the pump current of the second-stage amplifiers. However, inconsistency can be found between two output channels. Therefore, when the laser's power is less than 80 mW during the evaporation process, it is regulated by AOMs with the servo loop. The lasers' power as a function of the modulating voltage that drives AOMs is shown in Fig. 6(b). The laser power of two channels shows the good consistence, and it can be controlled precisely with the servo loop. In addition, the switch-off time of the laser system is less than 200 μs, which is achieved by both the AOM and the second-stage amplifier.

It is imperative that the amplifier requires sufficient optical input power when it is activated. In order to operate amplifier safely, the power sampling devices are placed behind all the

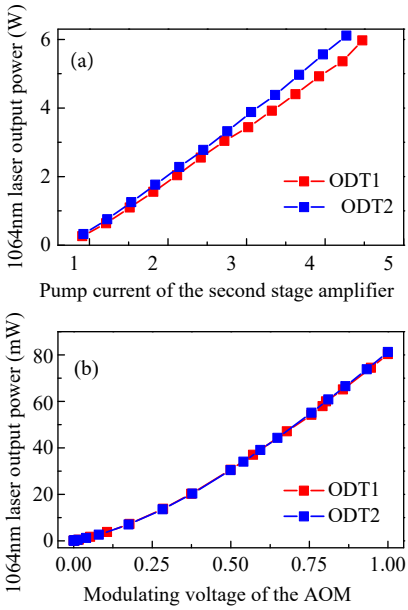

Fig. 6. (a) Output power of the 1064 nm laser system versus injected current into the YDFA. (b) Output power of the 1064 nm laser system in the servo loop as function of the modulating voltage, which drives AOMs.

active optical devices in the 1064 nm laser system, including the seeding source, YDF 1, YDF 2, YDF 3, and two AOMs (only the power sampling devices of the second-stage amplifiers are shown in Fig. 5) so that we can judge the states of the system and make the decision whether to turn on the current or not. Furthermore, the monitors are necessary for the on-orbit performance evaluation of all optical components.

5. REALIZATION OF THE ALL-OPTICAL ^{87}Rb BEC

The performance of the all-fiber laser system was validated by preparing the all-optical ^{87}Rb BEC.

The 780 nm laser system has the ability to cool atoms below the Doppler temperature limit, which is a suitable starting condition for ODT and evaporation. In our experiment, at

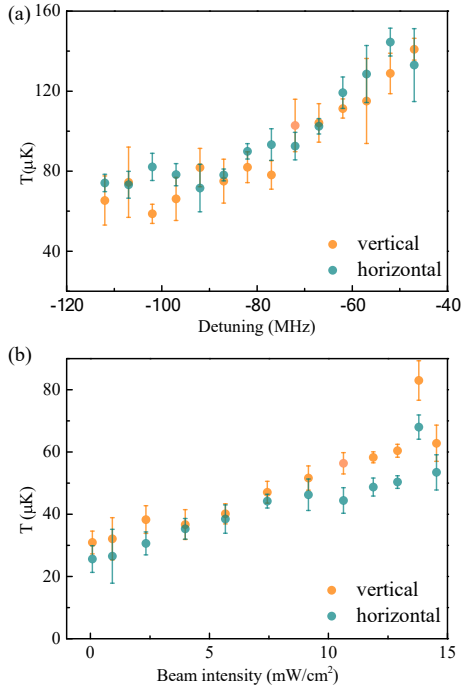

Fig. 7. (a) Temperature of the molasses as the function of the frequency detuning δ of the cooling laser. (b) Temperature of the molasses as the function of the 3D-MOT cooling laser beam intensity.

first, more than 1.5×10^9 atoms can be trapped in the 3D-MOT by optimizing the intensity and frequency of the 780 nm laser system. The optimized beam intensity and detuning of the 3D-MOT cooling laser is 14.5 mW/cm^2 and −18 MHz, respectively, and the beam intensity of the repumping laser is 4.4 mW/cm^2. Next, a compressed MOT stage and a temporal dark MOT (TDM) is executed after 3D-MOT for higher atomic density. The TDM was realized by decreasing the intensity of repumping laser, which is controlled by the AOM (193 MHz) in the optical control system. During the molasses phase, the atoms' temperature is further decreased by adjusting the detuning and the beam intensity of the cooling lasers. As shown in Fig. 7(a), the molasses's temperature decreases with larger detuning of the cooling laser, and the minimum temperature is 58.71(±4.80) μK and 82.11(±6.80) μK along the x and y direction. Maintaining the detuning at −102 MHz, the atom temperature can be decreased further by reducing the beam intensity. As a result, the cooling laser beam intensity is decreased to 0.077 mW/cm^2, and the lowest temperatures in horizontal and vertical directions are 30.94(±3.65) μK and 25.61(±4.29) μK, respectively, which is much lower than the Doppler limit.

The ability of the 1064 nm laser system was verified by loading more than 3×10^6 atoms in the ODT and evaporating them to BEC. The scheme of the crossed-ODT, which is shown in the inset of Fig. 8(a), consists of two 1064 nm laser beams that are parallel to the horizontal plane and crossed at the center of the science chamber. The waist diameter of the ODT laser beam is 60 μm, and their cross angle is 60°.

The evaporative cooling process lasts for 11181 ms, and the curve of the 1064 nm laser power during forced evaporation is shown in Fig. 8(a). With the effective forced evaporation, a "pure" condensate with roughly 1.2×10^5 atoms was acquired while the ODT power is being ramped down to 24 mW. As displayed in Fig. 8(b), the expansion of the BEC was detected by varying the TOF time t from 0 ms to 30 ms. Deduced from the expansion of the BEC [19], the effective kinetic energy temperature of the BEC is 72.69 (±8.7) nK and 25.15 (±3.2) nK along the x and y direction. In addition, the anisotropic expansion of the atom cloud proves the realization of the BEC. Here, we present the aspect ratio of atom cloud during the free expansion, as shown at the bottom right in Fig. 8(b).

To summarize, the performance of the all-fiber laser system we described in this paper, with the elaborate design and manufacture of the laser and its control strategy, can meet all experimental requirements for preparing an all-optical BEC.

6. CONCLUSION

In summary, a fiber laser system for preparing the all-optical ^{87}Rb BEC has been developed and deployed in the CSS since

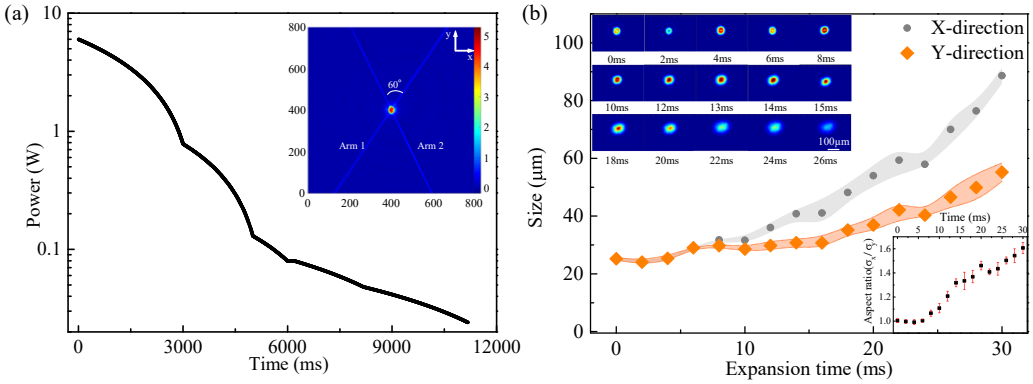

Fig. 8. (a) 1064 nm laser power as a function of time during the evaporation. The inset shows the absorptive images (false-color) of atoms trapped in the optical dipole trap corresponding the areas of 800 × 800 pixels (1.725 mm × 1.725 mm). (b) Size of the atomic cloud as a function of the expansion time in the x-y plane. The gray dots and yellow dots represent the 1/e widths of Gauss fits to the absorption images of the atomic cloud along the x and y axes, respectively. Limited to the initial spatial distribution and blurring during the different TOF time, a least-squares fit of the gauss functions gives $R^2 = 0.9$. The top-left inset shows typical absorption images in TOF measurement, and the scale bar corresponds to 100 μm. The bottom-right inset shows the aspect ratio of the BEC by varying the TOF time.

November 2022. The functional characterization of the all-fiber laser system, including the 780 nm laser system, optical control system, and 1064 nm laser system, is demonstrated by achieving BEC on ground. The high-power, single-frequency 780 nm fiber laser system is capable of atom cooling, capturing, and detecting. The power tracking modules effectively mitigate the power and polarization fluctuations in 780 nm PM fused fiber devices, resulting in a reduction of the power ratio between counter-propagating 3D-MOT cooling laser to 1.00385 within an hour. The 780 nm laser system and the optical control module enable the sub-Doppler cooling of ^{87}Rb atoms to 30 μK. The 1064 nm fiber laser system, featuring high-power, flexibility, and exceptional stability, has been developed and validated by effective loading and evaporative cooling in the ODT using a two-stage YDFA. The all-fiber laser system utilized in CAPR has demonstrated the capability of realizing an all-optical BEC, bridging the gap in utilizing all-fiber laser systems for preparing quantum degenerate gases. This all-fiber laser system, which is compact and highly reliable, provides an alternative solution for trapping and manipulating ultra-cold atoms in challenging environmental conditions.

Funding. China Manned Space Engineering Office; Chinese Academy of Sciences

Acknowledgment. The authors thank Wenli Wang, Yong Qian, Shuyu Zhou, Yu Xie, Angang Liang, and Mingshan Huang for their contributions to this work. The authors also thank the contributions from Lijia Wang, Yuanyuan Liu, Kedi Xie, Shuang Tang, Guibing Wang, Liping Chen, Zhichao Xing, Minghui Wen, Fenhong Song, Jianxin Huang, Aoqi Zhu, Aijun Zeng, Rui Li, Taijun Pan, Xin Zhou, Hongxin Liu, Hongwei Luo, Yiyan Yu, Shengnan Hu, Xingchen Wan, Wei Shi, and Pengfei Li.

Disclosures. The authors declare no conflicts of interest.

Data availability. Data underlying the results presented in this paper are not publicly available at this time but may be obtained from the authors upon reasonable request.

REFERENCES

1. M. H. Anderson, J. R. Ensher, M. R. Matthews, C. E. Wieman, and E. A. Cornell, "Observation of Bose-Einstein condensation in a dilute atomic vapor," Science **269**, 198–201 (1995).
2. K. B. Davis, M. Mewes, M. R. Andrews, N. J. van Druten, D. S. Durfee, D. M. Kurn, and W. Ketterle, "Bose-Einstein condensation in a gas of sodium atoms," Phys. Rev. Lett. **75**, 3969–3973 (1995).
3. C. C. Bradley, C. A. Sackett, J. J. Tollett, and R. G. Hulet, "Evidence of Bose-Einstein condensation in an atomic gas with attractive interactions," Phys. Rev. Lett. **75**, 1687–1690 (1995).
4. M. D. Barrett, J. A. Sauer, and M. S. Chapman, "All-optical formation of an atomic Bose-Einstein condensate," Phys. Rev. Lett. **87**, 010404 (2001).
5. M. Kozuma, L. Deng, E. W. Hagley, J. Wen, R. Lutwak, K. Helmerson, S. L. Rolston, and W. D. Phillips, "Coherent splitting of Bose-Einstein condensed atoms with optically induced Bragg diffraction," Phys. Rev. Lett. **82**, 871–875 (1999).
6. Y. Torii, Y. Suzuki, M. Kozuma, T. Sugiura, T. Kuga, L. Deng, and E. W. Hagley, "Mach-Zehnder Bragg interferometer for a Bose-Einstein condensate," Phys. Rev. A **61**, 041602 (2000).
7. M. P. A. Fisher, P. B. Weichman, G. Grinstein, and D. S. Fisher, "Boson localization and the superfluid-insulator transition," Phys. Rev. B **40**, 546–570 (1989).
8. T. Weber, J. Herbig, M. Mark, H. C. Nagerl, and R. Grimm, "Bose-Einstein condensation of cesium," Science **299**, 232–235 (2003).
9. G. Roati, C. D'Errico, L. Fallani, M. Fattori, C. Fort, M. Zaccanti, G. Modugno, M. Modugno, and M. Inguscio, "Anderson localization of a non-interacting Bose-Einstein condensate," Nature **453**, 895–898 (2008).
10. O. Zobay and B. M. Garraway, "Two-dimensional atom trapping in field-induced adiabatic potentials," Phys. Rev. Lett. **86**, 1195–1198 (2001).
11. E. A. Cornell and C. E. Wieman, "Nobel lecture: Bose-Einstein condensation in a dilute gas, the first 70 years and some recent experiments," Rev. Mod. Phys. **74**, 875–893 (2002).
12. A. E. Leanhardt, T. A. Pasquini, M. Saba, A. Schirotzek, Y. Shin, D. Kielpinski, D. E. Pritchard, and W. Ketterle, "Cooling Bose-Einstein condensates below 500 picokelvin," Science **301**, 1513–1515 (2003).
13. N. Gaaloul, M. Meister, R. Corgier, A. Pichery, P. Boegel, W. Herr, H. Ahlers, E. Charron, J. R. Williams, R. J. Thompson, W. P. Schleich, E. M. Rasel, and N. P. Bigelow, "A space-based quantum gas laboratory at picokelvin energy scales," Nat. Commun. **13**, 7889 (2022).
14. A. Vogel, M. Schmidt, K. Sengstock, *et al.*, "Bose-Einstein condensates in microgravity," Appl. Phys. B **84**, 663–671 (2006).
15. B. Barrett, L. Antoni-Micollier, L. Chichet, B. Battelier, T. Leveque, A. Landragin, and P. Bouyer, "Dual matter-wave inertial sensors in weightlessness," Nat. Commun. **7**, 13786 (2016).
16. T. van Zoest, N. Gaaloul, Y. Singh, *et al.*, "Bose-Einstein condensation in microgravity," Science **328**, 1540–1543 (2010).
17. D. Becker, M. D. Lachmann, S. T. Seidel, *et al.*, "Space-Borne Bose-Einstein condensation for precision interferometry," Nature **562**, 391–395 (2018).
18. G. Condon, M. Rabault, B. Barrett, L. Chichet, R. Arguel, H. Eneriz-Imaz, D. Naik, A. Bertoldi, B. Battelier, P. Bouyer, and A. Landragin, "All-optical Bose-Einstein condensates in microgravity," Phys. Rev. Lett. **123**, 240402 (2019).
19. D. C. Aveline, J. R. Williams, E. R. Elliott, C. Dutenhoffer, J. R. Kellogg, J. M. Kohel, N. E. Lay, K. Oudrhiri, R. F. Shotwell, N. Yu, and R. J. Thompson, "Observation of Bose-Einstein condensates in an Earth-orbiting research lab," Nature **582**, 193–197 (2020).
20. R. A. Carollo, D. C. Aveline, B. Rhyno, S. Vishveshwara, C. Lannert, J. D. Murphree, E. R. Elliott, J. R. Williams, R. J. Thompson, and N. Lundblad, "Observation of ultracold atomic bubbles in orbital microgravity," Nature **606**, 281–286 (2022).
21. D. O. Sabulsky, J. Junca, G. Lefevre, X. Zou, A. Bertoldi, B. Battelier, M. Prevedelli, G. Stern, J. Santoire, Q. Beaufils, R. Geiger, A. Landragin, B. Desruelle, P. Bouyer, and B. Canuel, "A fibered laser system for the MIGA large scale atom interferometer," Sci. Rep. **10**, 3268 (2020).
22. K. Frye, S. Abend, W. Bartosch, *et al.*, "The Bose-Einstein condensate and cold atom laboratory," EPJ Quantum Technol. **8**, 1 (2021).
23. W. Ren, Y. G. Sun, B. Wang, W. B. Xia, Q. Z. Qu, J. F. Xiang, Z. R. Dong, D. S. Lu, and L. Liu, "Highly reliable optical system for a rubidium space cold atom clock," Appl. Opt. **55**, 3607–3614 (2016).
24. L. Liu, D. S. Lu, W. B. Chen, *et al.*, "In-orbit operation of an atomic clock based on laser-cooled Rb-87 atoms," Nat. Commun. **9**, 2760 (2018).
25. M. Mihm, J. P. Marburger, A. Wenzlawski, O. Hellmig, O. Anton, K. Doringshoff, M. Krutzik, A. Peters, P. Windpassinger, and M. Team, "ZERODUR (R) based optical systems for quantum gas experiments in space," Acta Astronaut. **159**, 166–169 (2019).
26. T. Leveque, L. Antoni-Micollier, B. Faure, and J. Berthon, "A laser setup for rubidium cooling dedicated to space applications," Appl. Phys. B **116**, 997–1004 (2014).
27. V. Menoret, R. Geiger, G. Stern, N. Zahzam, B. Battelier, A. Bresson, A. Landragin, and P. Bouyer, "Dual-wavelength laser source for onboard atom interferometry," Opt. Lett. **36**, 4128–4130 (2011).
28. S. Kulas, C. Vogt, A. Resch, *et al.*, "Miniaturized lab system for future cold atom experiments in microgravity," Microgravity Sci. Technol. **29**, 37–48 (2017).
29. G. Stern, B. Allard, M. Robert-de-Saint-Vincent, J. P. Brantut, B. Battelier, T. Bourdel, and P. Bouyer, "Frequency doubled 1534 nm laser system for potassium laser cooling," Appl. Opt. **49**, 3092–3095 (2010).

30. S. S. Sane, S. Bennetts, J. E. Debs, C. C. N. Kuhn, G. D. McDonald, P. A. Altin, J. D. Close, and N. P. Robins, "11 W narrow linewidth laser source at 780 nm for laser cooling and manipulation of rubidium," Opt. Express **20**, 8915–8919 (2012).
31. C. Cherfan, M. Denis, D. Bacquet, M. Gamot, S. Zemmouri, I. Manai, J. F. Clement, J. C. Garreau, P. Szriftgiser, and R. Chicireanu, "Multi-frequency telecom fibered laser system for potassium laser cooling," Appl. Phys. Lett. **119**, 204001 (2021).
32. R. J. Thompson, M. Tu, D. C. Aveline, N. Lundblad, and L. Maleki, "High power single frequency 780 nm laser source generated from frequency doubling of a seeded fiber amplifier in a cascade of PPLN crystals," Opt. Express **11**, 1709–1713 (2003).
33. F. Theron, Y. Bidel, E. Dieu, N. Zahzam, M. Cadoret, and A. Bresson, "Frequency-doubled telecom fiber laser for a cold atom interferometer using optical lattices," Opt. Commun. **393**, 152–155 (2017).
34. F. Lienhart, S. Boussen, O. Carraz, N. Zahzam, Y. Bidel, and A. Bresson, "Compact and robust laser system for rubidium laser cooling based on the frequency doubling of a fiber bench at 1560 nm," Appl. Phys. B **89**, 177–180 (2007).
35. R. Geiger, V. Menoret, G. Stern, N. Zahzam, P. Cheinet, B. Battelier, A. Villing, F. Moron, M. Lours, Y. Bidel, A. Bresson, A. Landragin, and P. Bouyer, "Detecting inertial effects with airborne matter-wave interferometry," Nat. Commun. **2**, 474 (2011).
36. V. Schkolnik, O. Hellmig, A. Wenzlawski, J. Grosse, A. Kohfeldt, K. Doringshoff, A. Wicht, P. Windpassinger, K. Sengstock, C. Braxmaier, M. Krutzik, and A. Peters, "A compact and robust diode laser system for atom interferometry on a sounding rocket," Appl. Phys. B **122**, 217 (2016).
37. A. N. Dinkelaker, M. Schiemangk, V. Schkolnik, A. Kenyon, K. Lampmann, A. Wenzlawski, P. Windpassinger, O. Hellmig, T. Wendrich, E. M. Rasel, M. Giunta, C. Deutsch, C. Kurbis, R. Smol, A. Wicht, M. Krutzik, and A. Peters, "Autonomous frequency stabilization of two extended-cavity diode lasers at the potassium wavelength on a sounding rocket," Appl. Opt. **56**, 1388–1396 (2017).
38. M. Lezius, T. Wilken, C. Deutsch, *et al.*, "Space-borne frequency comb metrology," Optica **3**, 1381–1387 (2016).
39. V. Schkolnik, K. Doringshoff, F. B. Gutsch, M. Oswald, T. Schuldt, C. Braxmaier, M. Lezius, R. Holzwarth, C. Kurbis, A. Bawamia, M. Krutzik, and A. Peters, "JOKARUS—design of a compact optical iodine frequency reference for a sounding rocket mission," EPJ Quantum Technol. **4**, 9 (2017).
40. K. Doringshoff, F. B. Gutsch, V. Schkolnik, C. Kurbis, M. Oswald, B. Probster, E. V. Kovalchuk, A. Bawamia, R. Smol, T. Schuldt, M. Lezius, R. Holzwarth, A. Wicht, C. Braxmaier, M. Krutzik, and A. Peters, "Iodine frequency reference on a sounding rocket," Phys. Rev. Appl. **11**, 054068 (2019).
41. M. D. Lachmann, H. Ahlers, D. Becker, *et al.*, "Ultracold atom interferometry in space," Nat. Commun. **12**, 1317 (2021).
42. D. C. Aveline, J. R. Williams, E. R. Elliott, C. Dutenhoffer, J. R. Kellogg, J. M. Kohel, N. E. Lay, K. Oudrhiri, R. F. Shotwell, N. Yu, and R. J. Thompson, "Observation of Bose-Einstein condensates in an Earth-orbiting research lab (vol 582, pg 193, 2020)," Nature **584**, E1 (2020).
43. E. R. Elliott, M. C. Krutzik, J. R. Williams, R. J. Thompson, and D. C. Aveline, "NASA's cold atom lab (CAL): system development and ground test status," NPJ Microgravity **4**, 16 (2018).
44. L. Li, W. Xiong, B. Wang, *et al.*, "The design, realization, and validation of the scheme for quantum degenerate research in microgravity," IEEE Photon. J. **15**, 7100508 (2023).
45. Y. Hong, X. Hou, D. Chen, C. Zhou, M. Huang, T. Song, G. Wang, J. Zhao, and W. Chen, "Research on frequency stabilization technology of modulation transfer spectroscopy based on Rb^{87}," Chin. J. Laser **48**, 2101003 (2021).